

Prediction of a low-temperature ferroelectric instability in antiphase domain boundaries of strontium titanate

Alexander K. Tagantsev

Laboratoire de Céramique, EPFL, CH-1015 Lausanne, Switzerland

Eric Courtens and Ludovic Arzel

Laboratoire des Verres, UMR 5587 CNRS, Université Montpellier II, Place Eugène Bataillon, 34095 Montpellier Cedex 5, France

(Received 8 June 2001; published 21 November 2001)

The structure of the antiphase domain boundaries of strontium titanate SrTiO_3 that exist at temperatures below the antiferrodistortive transition, is analyzed. It is found that some boundaries are similar to Néel domain walls, as an additional component of the order parameter develops within them. We show quantitatively that at low temperatures, typically below ~ 40 K, such boundaries become unstable with respect to the development of a ferroelectric polarization. This ferroelectric transition might provide the much needed explanation for several anomalies that are experimentally observed in SrTiO_3 in this temperature region.

DOI: 10.1103/PhysRevB.64.224107

PACS number(s): 77.84.Dy, 68.35.-p, 77.80.Dj, 81.30.-t

I. INTRODUCTION

Perovskites ABO_3 can undergo several types of crystal-line instabilities at different points of their Brillouin zone (BZ).¹ In particular there are structural ones, often related to rotations of BO_6 octahedra, and there are ferroelectric ones, mostly due to the polar displacement of the B -site ion. Which of these dominates depends on the so-called “tolerance factor” t that describes the relative filling of space by the various ions.² If the radius of A is too small ($t < 1$) the structural instability is generally observed, while if B is too small ($t > 1$) ferroelectricity can be favored.

Strontium titanate, SrTiO_3 , is an interesting case where $t \approx 1$ and in which both types of instabilities can be simultaneously active. The crystal is simple cubic $Pm\bar{3}m$ at room temperature. On cooling, SrTiO_3 first undergoes an antiferrodistortive structural transition at $T_a \approx 105$ K. It is due to static octahedra rotations around one cubic axis, the rotations alternating from cell to cell in all three cubic directions.^{3,4} Hence, this transition occurs at the R point of the BZ. Below T_a , the symmetry is tetragonal, $I4/mcm$, where the tetragonal axis \vec{c} is parallel to the octahedron-rotation axis. The transition is accompanied by the development of small but physically important spontaneous strains.⁵ On the other hand, the ferroelectric instability manifests itself by large dielectric constants, which become anisotropic and continue to increase below T_a to saturate at low temperatures T , with $\epsilon_a \approx 40\,000$ in the ab plane and $\epsilon_c \approx 10\,000$ along the \vec{c} axis.⁶⁻⁸ In this regime, the lattice vibrations are nonclassical, which leads to a strong departure from the Curie-Weiss law.⁸ However, this fact alone is not sufficient to prevent the ferroelectric transition. The actual suppression of ferroelectricity is due to the competition between the structural order parameter and the ferroelectric one.⁹ It was shown recently that if just the spontaneous strains associated with the transition could somehow be prevented, a ferroelectric transition would actually take place.¹⁰

Strong changes of the structural order parameter can occur locally in the regions separating different structural do-

main. Naively one might think that the structural order parameter could pass through zero in the middle of such “walls.” Specifically, something similar to this might happen for the so-called “antiphase domain boundaries,” since the order parameter changes sign between two such domains, as opposed to “twin walls” where it simply changes direction. Hence, one might expect that under favorable conditions the ferroelectric instability could be restored within an antiphase boundary, as most strains are fixed by the adjacent bulk domains, while the structural order parameter is strongly perturbed inside the boundary.

The study of such instabilities is the subject of this paper. We are motivated in this by the observation of various unexplained phenomena at low temperatures in SrTiO_3 , as partly reviewed in Ref. 11. In particular, Müller and collaborators have reported the EPR observation of a transitionlike anomaly at a temperature $T_q \approx 37$ K.¹² This value is close to that of the *bare* ferroelectric instability, i.e., the one which is not renormalized by interactions with the structural distortions, which occurs near 30 K.¹⁰ Recent investigations of the “Müller state” suggested that its existence might be quite sensitive to sample preparation and history.¹³ An explanation in terms of antiphase boundaries would account for this somewhat elusive nature of the phenomenon. Another issue of interest is the strong anomaly that is observed at similar temperatures in the dielectric losses of SrTiO_3 .^{14,15} Finally, the influence of antiphase domain boundaries has also been invoked to account more generally for anomalous neutron-scattering spectra.¹³ For all these reasons it appears useful to perform such an analysis, this all the more that the necessary parameters are quite well known for SrTiO_3 .^{7,16,17,10}

The theoretical treatment will be performed in the continuous approximation whose validity will be justified *a posteriori*. In this spirit, we shall use a Gibbs potential similar to that first introduced by Uwe and Sakudo,⁷ but including also the gradient terms as done by Cao and Barsch.¹⁸ This is defined in Sec. II where an example is given for the calculation of a possible order-parameter profile in an antiphase boundary. The stability of such boundaries with respect to the appearance of other components of the structural order

parameter is discussed in Sec. III, where it is found that the really stable solution can indeed be more complicated. Section IV then discusses the stability of these antiphase boundaries with respect to the development of polarization components. We do find that a ferroelectric transition can occur for boundaries of particular orientations. The potential relevance of this phenomenon to the low-temperature anomalies of SrTiO₃ is discussed in Sec. V. A summary concludes the paper.

II. GIBBS POTENTIAL AND CALCULATION OF A SIMPLE ORDER-PARAMETER PROFILE

The structural order parameter is an axial vector $\vec{\phi}$. Its three components are the values of the staggered rotation angles of the oxygen octahedra around the three cubic axes ϕ_i ($i=1$ to 3). In SrTiO₃ under normal conditions, below T_a the ferroic phase exhibits six tetragonal domain states in which the order parameter is $(\phi_0 \ 0 \ 0)$, $(-\phi_0 \ 0 \ 0)$, $(0 \ \phi_0 \ 0)$, etc. Here ϕ_0 is the value of the spontaneous

rotation, which is measured by the displacement of an appropriate O atom from its cubic position as defined by Uwe and Sakudo.⁷ The domain boundaries separating states which differ only by the sign of ϕ_0 are called ‘‘antiphase’’ ones. Such states have a common tetragonal axis and they are macroscopically indistinguishable because a sign change of ϕ_0 corresponds to a translation by just one lattice constant of the parent phase.

The question of the structure of an antiphase boundary in SrTiO₃ was already addressed by Cao and Barsch.¹⁸ They used an approach due to Zhirnov¹⁹ to calculate the order-parameter profile for a particular orientation of the boundary. We employ the same method to calculate other boundary orientations, as well as to determine the stability of these boundaries. In contrast to Cao and Barsch, we base the calculation on the elastic Gibbs function G rather than on the Helmholtz one, as it simplifies the derivations. The part of the Gibbs function containing the order parameter and the mechanical stresses σ_i in contracted notation²⁰ is written

$$\begin{aligned}
 G_\phi = & b_1(\phi_1^2 + \phi_2^2 + \phi_3^2) + b_{11}(\phi_1^4 + \phi_2^4 + \phi_3^4) + b_{12}(\phi_1^2\phi_2^2 + \phi_2^2\phi_3^2 + \phi_3^2\phi_1^2) - \frac{1}{2}s_{11}(\sigma_1^2 + \sigma_2^2 + \sigma_3^2) - s_{12}(\sigma_1\sigma_2 + \sigma_2\sigma_3 + \sigma_3\sigma_1) \\
 & - \frac{1}{2}s_{44}(\sigma_4^2 + \sigma_5^2 + \sigma_6^2) - R_{11}(\phi_1^2\sigma_1 + \phi_2^2\sigma_2 + \phi_3^2\sigma_3) - R_{12}[(\phi_2^2 + \phi_3^2)\sigma_1 + (\phi_3^2 + \phi_1^2)\sigma_2 + (\phi_1^2 + \phi_2^2)\sigma_3] \\
 & - R_{44}(\phi_2\phi_3\sigma_4 + \phi_3\phi_1\sigma_5 + \phi_1\phi_2\sigma_6) + \frac{1}{2}\delta_{11}[(\partial\phi_1/\partial x_1)^2 + (\partial\phi_2/\partial x_2)^2 + (\partial\phi_3/\partial x_3)^2] + \delta_{12}[(\partial\phi_1/\partial x_1)(\partial\phi_2/\partial x_2) \\
 & + (\partial\phi_2/\partial x_2)(\partial\phi_3/\partial x_3) + (\partial\phi_3/\partial x_3)(\partial\phi_1/\partial x_1)] + \frac{1}{2}\delta_{44}[(\partial\phi_1/\partial x_2 + \partial\phi_2/\partial x_1)^2 + (\partial\phi_2/\partial x_3 + \partial\phi_3/\partial x_2)^2 \\
 & + (\partial\phi_3/\partial x_1 + \partial\phi_1/\partial x_3)^2], \tag{1}
 \end{aligned}$$

where the x_j 's are the Cartesian coordinates. For all second and fourth rank tensors we will be using the Voigt notation ($j=1$ to 6) unless specified otherwise. From G , one obtains the equations of state

$$\frac{\partial}{\partial x_i}[\partial G/\partial(\partial\phi_j/\partial x_i)] = \partial G/\partial\phi_j \quad (j=1 \text{ to } 3), \tag{2}$$

and the constitutive equations of elasticity

$$\varepsilon_k = -\partial G/\partial\sigma_k, \tag{3}$$

where the strains ε_k must satisfy the Saint-Venant compatibility conditions.²¹ In Eq. (2), as well as below, the summation over repeated indices is implied. Following the standard practice, for a boundary which is perpendicular to x_1 , we set $\sigma_1 = \sigma_5 = \sigma_6 = 0$, which assumes that no longitudinal stress and no transverse shears are applied to this boundary. This is compatible with the conditions $\partial\sigma_{ij}/\partial x_j = 0$ ($i, j=1$ to 3). The strains ε_2 , ε_3 , and ε_4 are independent of the coordinates

and fixed by the spontaneous strains in the bulk far from the boundary, while ε_1 , ε_5 , and ε_6 are x_1 dependent and satisfy the Saint-Venant conditions.

There are two extreme orientations of the antiphase-boundary planes with respect to the tetragonal axis. Those which are orthogonal to \vec{c} shall be called ‘‘longitudinal’’ as their normal is $\parallel\vec{c}$. Those which contain \vec{c} shall be called ‘‘transversal’’ as their normal is $\perp\vec{c}$. Considering just the rigidity of the oxygen octahedra TiO₆, one observes that longitudinal boundaries, which are parallel to the ab plane, could be drawn infinitely thin, cutting the structure at the height of the undisplaced apex oxygens. This produces no disruption in the oxygen positions and no distortions of the oxygen octahedra. Hence, such boundaries should occur fairly easily and they are indeed likely to be rather thin. They could as well be called ‘‘easy’’ boundaries. They were the ones considered in Ref. 18. On the other hand, transverse boundaries cannot be drawn without severe distortions of the octahedra, with alternate elongations and compressions of the O-O distances. Therefore they are likely to be rather

energetic and thick, and they could also be called “hard.” This intuitive reasoning is fully confirmed by the detailed calculations presented below.

For illustration, a continuous calculation for a transverse boundary is now presented in some details. The bulk order parameter is taken along the third axis, $\phi_3 = \pm \phi_0$, and the boundary plane is momentarily selected to be perpendicular to the first axis. We assume in this section that no new component of the order parameter develops within the boundary. Boundaries with that property will thereafter be called “simple.” From Eq. (2), with $j=3$, one obtains

$$\delta_{44}\partial^2\phi_3/\partial x_1^2 = 2b_1\phi_3 + 4b_{11}\phi_3^3 - 2[R_{11}\sigma_3 + R_{12}(\sigma_1 + \sigma_2)]\phi_3. \quad (4)$$

From Eq. (3), one finds

$$\begin{aligned} \varepsilon_1 &= s_{11}\sigma_1 + s_{12}(\sigma_2 + \sigma_3) + R_{12}\phi_3^2, \\ \varepsilon_2 &= s_{11}\sigma_2 + s_{12}(\sigma_1 + \sigma_3) + R_{12}\phi_3^2, \\ \varepsilon_3 &= s_{11}\sigma_3 + s_{12}(\sigma_1 + \sigma_2) + R_{11}\phi_3^2, \\ \varepsilon_k &= s_{44}\sigma_k \quad (k=4 \text{ to } 6). \end{aligned} \quad (5)$$

In this case ε_2 and ε_3 are fixed by bulk values. For the bulk, $\sigma_i=0$ ($i=1$ to 6), so that Eqs. (5) give

$$\begin{aligned} \varepsilon_2 &= R_{12}\phi_0^2, \\ \varepsilon_3 &= R_{11}\phi_0^2, \end{aligned} \quad (6)$$

while ε_4 to ε_6 are zero. The value of ϕ_0 results from Eq. (4),

$$\phi_0 = \pm \sqrt{-b_1/2b_{11}}. \quad (7)$$

The stress-free condition of the boundary is simply $\sigma_1=0$. Eliminating σ_2 and σ_3 between Eqs. (4) and (5) one arrives at

$$-\delta_{44}\partial^2\phi_3/\partial x_1^2 + B_e^0(2b_1\phi_3 + 4b_{11}\phi_3^3) = 0, \quad (8)$$

where B_e^0 is given by

$$B_e^0 = 1 + \frac{1}{4b_{11}} \left[\frac{(R_{11} + R_{12})^2}{s_{11} + s_{12}} + \frac{(R_{11} - R_{12})^2}{s_{11} - s_{12}} \right]. \quad (9)$$

In the absence of mechanical coupling one would just have $B_e^0=1$. The solution of Eq. (8) which satisfies the boundary condition can be written

$$\begin{aligned} \phi_3(x_1) &= \phi_0 \tanh(x_1/t_w), \\ t_w &= t_0/\sqrt{B_e^0}, \\ t_0 &= \sqrt{-\delta_{44}/b_1}. \end{aligned} \quad (10)$$

The value t_0 is the boundary half-width in the absence of mechanical effects. Calculating the difference between the value of G_ϕ obtained in the presence of one such boundary and the homogeneous value of G_ϕ , one obtains the excess boundary energy per unit area. It is given by

$$G_w = G_{w0}\sqrt{B_e^0},$$

$$G_{w0} = (2\sqrt{2}/3)\phi_0^3\sqrt{4b_{11}\delta_{44}}. \quad (11)$$

The above results can easily be generalized to any transverse boundary forming an angle α with the second axis. In a reference frame rotated around x_3 , let the axis x'_1 be perpendicular to the boundary. The equation of state (4) is unmodified, with x_1 simply replaced by x'_1 , while all stresses are expressed in the original reference frame. Solving the elastic problem in that more general case, one finds that all above results remain, except for the replacement of B_e^0 by a more general expression

$$B_e^\alpha = 1 + \frac{1}{2b_{11}}[R_{11}\Xi_3 + R_{12}\Xi_{1,2}], \quad (12)$$

where the coefficients Ξ_i relate to the stresses $\{\sigma_i\}_m$ in the middle of the boundary (where $\phi_3=0$) by

$$\begin{aligned} \{\sigma_1 + \sigma_2\}_m &= \Xi_{1,2}\phi_0^2, \\ \{\sigma_3\}_m &= \Xi_3\phi_0^2. \end{aligned} \quad (13)$$

The value of the coefficients Ξ_i is given by

$$\begin{aligned} \Xi_{1,2} &= -\frac{1}{\Delta} \left[\sin^2 2\alpha + \frac{s_{44} \cos^2 2\alpha}{2(s_{11} - s_{12})} \right] \frac{s_{12}R_{11} - s_{11}R_{12}}{s_{11}}, \\ \Xi_3 &= -\frac{s_{12}}{s_{11}}\Xi_{1,2} + \frac{R_{11}}{s_{11}}, \\ \Delta &= \sin^2 2\alpha \left[\frac{1}{2}(s_{11} + s_{12}) + \frac{1}{4}s_{44} - \frac{s_{12}^2}{s_{11}} \right] \\ &\quad + \cos^2 2\alpha \frac{(s_{11} + s_{12})s_{44}}{2s_{11}}. \end{aligned} \quad (14)$$

In the case of the longitudinal boundary, which is perpendicular to x_3 , the left side of Eq. (4) is replaced by $\delta_{11}\partial^2\phi_3/\partial x_3^2$, and nothing else is changed, except for the boundary conditions which now read $\sigma_3=0$ and $\varepsilon_1=\varepsilon_2=R_{12}\phi_0^2$. One arrives at Eq. (10) with B_e^0 replaced by

$$B_e^l = 1 + \frac{R_{12}^2}{b_{11}(s_{11} + s_{12})} \quad (15)$$

and δ_{44} replaced by δ_{11} , so that

$$t_0 = \sqrt{-\delta_{11}/b_1}. \quad (16)$$

The same replacements must be made in G_{w0} in Eq. (11). Since $\delta_{11} \ll \delta_{44}$ (Appendix), the “easy” boundaries are indeed much less energetic than the “hard” ones. The above results on the longitudinal boundaries are equivalent to those of Cao and Barsch,¹⁸ except for the different notations.

The parameters that allow one to evaluate these expressions have all been quite well determined. The specific numerical values used for the purpose of this paper are listed in the Appendix. With these, one can calculate the mechanical

correction factors $B_e - 1$ of Eqs. (9), (12), and (15). One finds in all cases that $B_e - 1 \sim 0.1$, hence these corrections are never large. Also, the angular anisotropy in Eq. (12) is very small, ~ 0.002 only. The main difference with the evaluation in Ref. 18 is in the size of the gradient terms that are needed to calculate the boundary thicknesses in Eqs. (10) and (16). We find that the values in Table IV of Ref. 18 should be multiplied by $4\pi^2$ in order to conform with the units used by Stirling.¹⁶ This gives boundary thicknesses that are 2π times larger than in Ref. 18. The full thickness of the longitudinal boundary (16) at 40 K is then $2t_w \approx 8 \text{ \AA}$. This is indeed very thin. That of the “simple” transverse boundary (10) is $2t_w \approx 44 \text{ \AA}$. While the former is somewhat small to guarantee the validity of a continuous approximation, the latter which amounts to $\sim 11a_0$, where a_0 is the lattice parameter, seems sufficient. Anticipating on the following sections, we shall see that while the longitudinal boundary is stable against the development of another component of $\vec{\phi}$, this is not the case for transverse boundaries. The latter then become thicker yet. Similarly the longitudinal boundary is stable against a polar instability, and thus the interest will concentrate on *thick transverse* boundaries. For these the continuous approximation is very well justified.

III. STRUCTURAL STABILITY OF ANTIPHASE BOUNDARIES AND CALCULATION OF A REAL PROFILE

In this section we consider the stability of the simple solutions obtained in Sec. II against the emergence of another component of the structural order parameter within the boundary. We find that while the easy boundaries are stable, the hard ones develop a component of $\vec{\phi}$ perpendicular to the boundary plane, similar to Néel walls in magnetism. The question of stability was addressed previously in the context of competing structural and magnetic instabilities²² and also for improper ferroelectrics.²³ The idea is to allow for a small perturbation of the wall and to study whether it lowers the energy. Mathematically, the small perturbation has to satisfy a wave equation which is the corresponding linearized equation of state. The associated eigenvalue enters into the calculation of the perturbed energy. The instability results from a negative eigenvalue.

We consider first the stability of the hard antiphase boundary described by Eqs. (8) and (10) against the development of an order-parameter component ϕ_1 . The equation of state linearized with respect to ϕ_1 reads

$$-\delta_{11}\partial^2\phi_1/\partial x_1^2 + 2b_1\phi_1 + 2b_{12}\phi_1\phi_3^2 - 2R_{11}\phi_1\sigma_1 - 2R_{12}\phi_1(\sigma_2 + \sigma_3) - R_{44}\phi_3\sigma_5 = 0, \quad (17)$$

where one can set $\sigma_1 = \sigma_5 = 0$ as explained above. In Eq. (17), ϕ_3 is given by Eq. (10) while a simple calculation gives $\sigma_2 + \sigma_3 = (\phi_0^2 - \phi_3^2)(\Xi_{1,2} + \Xi_3)$, as in Eqs. (13) and (14) with $\alpha = 0$. Equation (17) is of the form $\hat{L}\phi_1 = 0$, where \hat{L} is the operator

$$\hat{L} \equiv -\delta_{11}\frac{d^2}{dx_1^2} + C + U \tanh^2\left(\frac{x_1}{t_w}\right), \quad (18)$$

with

$$U = \left[2b_{12} + 2R_{12}\frac{R_{11} + R_{12}}{s_{11} + s_{12}} \right] \phi_0^2, \\ C = \left[-4b_{11} - 2R_{12}\frac{R_{11} + R_{12}}{s_{11} + s_{12}} \right] \phi_0^2. \quad (19)$$

The instability of the wall results from a negative eigenvalue λ for the operator \hat{L} .^{22,24} The eigenvalues of Eq. (18) are known.²⁵ The lowest one is

$$\lambda = \frac{\sqrt{1 + 4Ut_w^2/\delta_{11}} - 1 + 2Ct_w^2/\delta_{11}}{2t_w^2/\delta_{11}}. \quad (20)$$

One should note that b_{12} must be positive, otherwise the ground state in the bulk is not the stable one. As the mechanical corrections in Eq. (19) are relatively small (as can be checked using the numerical values in the Appendix), U is positive. This shows that a necessary condition for the instability is $C < 0$, which implies that the equation of state is already unstable at the center of the boundary where $x_1 = 0$. The condition for the instability of the boundary, $\lambda < 0$, can be rewritten

$$U + C < C^2 t_w^2 / \delta_{11}. \quad (21)$$

As $t_w^2 \propto \delta_{44}$, the quantity t_w^2/δ_{11} involves the ratio δ_{44}/δ_{11} which is very large (see the Appendix). As a result, the evaluation of Eq. (21) using Eq. (19) leads for this transverse boundary to an instability against the appearance of a component of the order parameter normal to the boundary plane.

The same result is obtained for all other transverse boundaries, i.e., for any value of the angle α introduced in the previous section. On the other hand, the stability condition for the longitudinal boundary involves the ratio δ_{11}/δ_{44} which is very small. For this reason one finds that simple longitudinal boundaries, with $\phi_1 = 0$ throughout, are stable at least within this continuous approximation.

We now turn to the actual profile of transverse boundaries. For simplicity we take the case $\alpha = 0$, and we first allow for $\phi_1 \neq 0$ within the boundary. Such a boundary is equivalent to a Néel wall in magnetism, as we now have two rotational components, ϕ_1 and ϕ_3 , where ϕ_1 is directed along the boundary thickness. For this kind of boundary, the equation for ϕ_3 is similar to Eq. (4), with just two additional terms containing ϕ_1 on the right-hand side (RHS): $2b_{12}\phi_1^2\phi_3 - R_{44}\sigma_5\phi_1$. The equation for ϕ_1 is similar to Eq. (17), but including the cubic term on the RHS: $4b_{11}\phi_1^3$. As done above, we set in these equations $\sigma_1 = \sigma_5 = 0$. The values of σ_2 and σ_3 should now be deduced from modified Eqs. (5) that make allowance for the nonzero component ϕ_1 :

$$\varepsilon_2 = s_{11}\sigma_2 + s_{12}(\sigma_1 + \sigma_3) + R_{12}(\phi_3^2 + \phi_1^2), \\ \varepsilon_3 = s_{11}\sigma_3 + s_{12}(\sigma_1 + \sigma_2) + R_{11}\phi_3^2 + R_{12}\phi_1^2, \quad (22)$$

where ε_2 and ε_3 are fixed by Eq. (6). Introducing these in the

equations for ϕ_1 and ϕ_3 , one obtains two coupled differential equations that can be written in terms of the reduced variables $\psi_1 \equiv \phi_1/\phi_0$ and $\psi_3 \equiv \phi_3/\phi_0$. Furthermore, these equations simplify by using distances scaled to t_w from Eq. (10), defining a reduced distance x by

$$x \equiv x_1/t_w. \quad (23)$$

The coupled nonlinear equations are then

$$\frac{1}{2} \mu \frac{\partial^2 \psi_1}{\partial x^2} = [-1 + \epsilon + (1 + \zeta)\psi_1^2 + (1 + \eta)\psi_3^2]\psi_1,$$

$$\frac{1}{2} \frac{\partial^2 \psi_3}{\partial x^2} = [-1 + (1 + \eta)\psi_1^2 + \psi_3^2]\psi_3, \quad (24)$$

where

$$\mu = \delta_{11}/\delta_{44}, \quad (25)$$

$$\eta = U/(4b_{11}\phi_0^2 B_e^0) - 1,$$

$$\epsilon = (b_{12} - 2b_{11})/(2b_{11}B_e^0) - \eta,$$

$$\zeta = B_e^l/B_e^0 - 1. \quad (26)$$

The values of B_e^0 , B_e^l , and U are given by Eqs. (9), (15), and (19), respectively. From the parameters in the Appendix, one calculates $\mu \approx 0.04$, $\eta \approx 0.042$, $\zeta \approx 0.037$, $\epsilon \approx 0.094$.

In general, the system of equations (24) can only be solved numerically. However, for this particular boundary there exists a physically justified approximation that provides for an analytical solution of the problem. A remarkable feature of the structural ordering in SrTiO_3 is its quasi-two-dimensional nature. The correlation of the oxygen-octahedra rotations is very anisotropic. For rotations around \vec{c} , it is strong within any given ab layer, whereas rotations in adjacent ab layers are only weakly coupled. This is manifested by the smallness of the parameter μ . The quasi-2D approximation $\mu = 0$ is made for the remainder of this section as it allows one to obtain this analytic solution.

Inspection of the above equations might suggest that elastic effects could be weak in this problem. If one makes the approximation $B_e^l = B_e^0 = 1$, the coefficients simplify considerably, with $\zeta = \epsilon = 0$ and $\eta = \eta_0 = -1 + b_{12}/(2b_{11}) \approx 0.149$. It is, however, known that in domain-wall problems the mechanical effects, although involving relatively small numerical coefficients, are often of principal importance. It is instructive to first neglect the mechanical effects which has the further merit to simplify the equations and thus the presentation. In a second step the mechanical effects are reintroduced to obtain the correct result, thereby showing the dramatic changes that they produce.

With $\mu = 0$, the first Eq. (24) splits into two branches. Without mechanical effects these are

$$\psi_1 = 0,$$

$$\psi_1^2 = 1 - (1 + \eta_0)\psi_3^2. \quad (27)$$

To produce a Néel wall, the second branch must apply, but ψ_1^2 cannot be negative so that there are *crossovers* to the first branch at $\psi_3^2 = 1/(1 + \eta_0)$. Both ends of the boundary profile, where ψ_3 is nearly 1, obey thus the equation

$$\frac{1}{2} \frac{\partial^2 \psi_3}{\partial x^2} = (\psi_3^2 - 1)\psi_3, \quad (28)$$

with $\psi_1 = 0$, while the central region obeys

$$\frac{1}{2} \frac{\partial^2 \psi_3}{\partial x^2} = \eta_0[\psi_3 - (2 + \eta_0)\psi_3^3], \quad (29)$$

with ψ_1 given by the second branch (27). The solution of Eq. (28) that satisfies the boundary conditions $\psi_3 = \pm 1$ at $x = \pm \infty$ is $\psi_3 = \tanh(x - x_0)$ where x_0 is a free parameter. To solve Eq. (29), a standard procedure (see, e.g., Ref. 26) is to remark that it has the structure of an equation of motion

$$\frac{m}{2} \ddot{\psi} = -\frac{\partial V}{\partial \psi}, \quad (30)$$

which integrates to

$$\frac{m}{2} \dot{\psi}^2 + V(\psi) = \text{const}, \quad (31)$$

where ψ is the coordinate of a particle in the potential $V(\psi)$ while x plays the role of time. The potential for the $\psi_1 = 0$ branch is simply

$$V(\psi_3) = \frac{1}{2} \psi_3^2 - \frac{1}{4} (1 + \psi_3^4), \quad (32)$$

where use was made of the free constant to arbitrarily set V to zero at $\psi_3^2 = \pm 1$. The structure of the system (24) is such that ψ , $\dot{\psi}$, and $\ddot{\psi}$ must be continuous at the crossover points. These matching conditions are then used to determine the value of the constant for the central segment of the potential for which one finds

$$V(\psi_3) = -\frac{\eta_0}{2} \psi_3^2 + \eta_0 \frac{2 + \eta_0}{4} \psi_3^4. \quad (33)$$

The potential $V(\psi_3)$ from Eqs. (32) and (33) is drawn in Fig. 1(a). The circles show the crossover points $\psi_3^2 = 1/(1 + \eta_0)$. The total potential separates into two distinct wells. A particle launched from $\psi_3 = -1$ at $x = -\infty$ with zero $\dot{\psi}$ will take an infinite ‘‘time’’ to reach $\psi_3 = 0$. In terms of space, this means that such a boundary would split into two infinitely separated twin walls, or in other words that there were no Néel antiphase boundary. This result is not consistent with

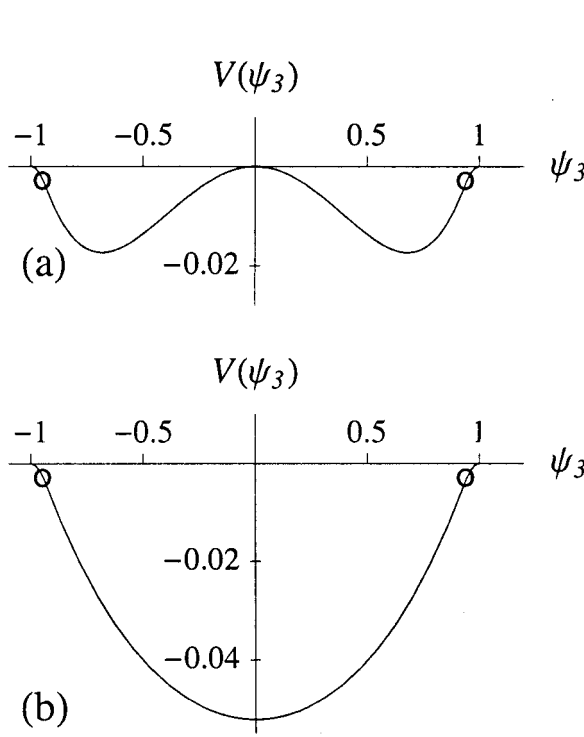


FIG. 1. The potential $V(\psi_3)$ that determines the profile of the Néel-type hard antiphase boundary perpendicular to the $\langle 100 \rangle$ direction in SrTiO₃: (a) with neglect of elastic effects [Eqs. (32) and (33)]; (b) with inclusion of the elastic effects [Eqs. (32) and (35)]. The open dots are located at the crossovers between the two branches of the solution.

the real situation of $\langle 100 \rangle$ -oriented twin boundaries in SrTiO₃. One can readily show that for this orientation the twin boundaries are mechanically incompatible.²⁷ Hence, the decay into separated twin boundaries is a clear consequence of the neglect of elastic effects.

Including the elastic effects, the crossover point between the two branches now occurs at $\psi_3^2 = (1 - \epsilon)/(1 + \eta)$. Following a similar reasoning, Eq. (29) is replaced by

$$\frac{1}{2} \frac{\partial^2 \psi_3}{\partial x^2} = \frac{\eta - \epsilon - \epsilon \eta - \zeta}{1 + \zeta} \psi_3 + \frac{\zeta - 2\eta - \eta^2}{1 + \zeta} \psi_3^3. \quad (34)$$

The numerical values of the coefficients on the RHS are -0.090 and -0.047 , respectively. The potential for the $\psi_1 = 0$ branch is still given by Eq. (32). The potential corresponding to Eq. (34) can be written

$$V(\psi_3) = 0.045\psi_3^2 + 0.0118\psi_3^4 - 0.052 = c(\psi_3^2 - a^2)(\psi_3^2 + b^2). \quad (35)$$

As above, the constant in $V(\psi_3)$ is obtained by matching the potential (35) at the crossover points with Eq. (32). The coefficients a^2 , b^2 , and c have numerical values of 0.93 , 4.75 , and 0.0118 , respectively. This potential is illustrated in Fig. 1(b). The major difference with Fig. 1(a) is in the sign of the quadratic term which is here positive. As a result the separa-

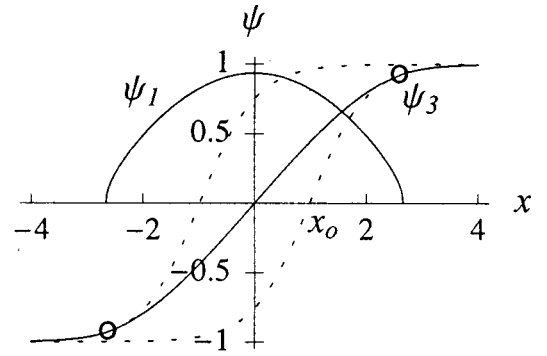


FIG. 2. The reduced order-parameter profiles $\psi_i = \phi_i / \phi_0$ ($i = 1, 3$) for the Néel-type boundary corresponding to case (b) in Fig. 1. The continuous lines show the solutions for ψ_1 and ψ_3 , with open dots showing the crossovers on ψ_3 . The dashed lines are the $\tanh(x \pm x_0)$ solutions that prolongate the solutions for ψ_3 obtained in the wings where $\psi_1 = 0$. The horizontal distance between these tanh solutions show the increase in wall thickness of ~ 2 reduced units owing to the presence of ψ_1 .

tion into two wells is removed. This is a remarkable manifestation of the major role of the “apparently weak” elastic terms. It reflects the aforementioned elastic incompatibility of the $\langle 100 \rangle$ twin walls. The equation resulting from Eqs. (30) and (35)

$$\frac{1}{4} \psi_3^2 + c(\psi_3^2 - a^2)(\psi_3^2 + b^2) = 0 \quad (36)$$

is integrable in terms of standard functions. The solution that satisfies the condition $\psi_3 = 0$ at $x = 0$ is

$$x = \frac{1}{2\sqrt{c}} \frac{1}{\sqrt{a^2 + b^2}} F(\gamma|m),$$

$$\gamma = \arcsin \frac{\psi}{a} \sqrt{\frac{a^2 + b^2}{\psi^2 + b^2}},$$

$$m = \frac{a^2}{a^2 + b^2}, \quad (37)$$

where $F(\gamma|m)$ is the elliptic integral of the first kind. It matches the solution for $\psi_1 = 0$, $\psi_3 = \tanh(x \pm x_0)$, at the crossover points with $x_0 = 0.985$. This solution is illustrated in Fig. 2 in which the tanh solutions have been continued by dashed lines whose separation illustrates the increase in wall thickness produced by the presence of the ψ_1 component. The value of ψ_1 is also drawn. One notices that in the middle of the boundary $\{\phi_1\}_m$ nearly reaches ϕ_0 ,

$$\{\phi_1^2\}_m = \phi_0^2(1 - \epsilon)/(1 + \zeta), \quad (38)$$

or $\{\phi_1\}_m = 0.935\phi_0$. This is close to a pure rotation of $\vec{\phi}$ as in magnetic Néel walls. The neglect of the second derivative of ψ_1 (having set $\mu=0$) is obviously a poor approximation in the region where there is a break in the ψ_1 curve. The presence of the term $\frac{1}{2}\mu\partial^2\psi_1/\partial x^2$ will effectively smooth that region. This term only has a minor effect in the center of the boundary. Indeed, dividing the first Eq. (24) by ψ_1 one observes that $\frac{1}{2}\mu(\partial^2\psi_1/\partial x^2)/\psi_1$ is well below one percent as opposed to the other terms of the order of 1 that are kept in that equation.

It remains to check for the stability of the Néel boundary against the development of the third component of the order parameter ϕ_2 . The linearized equation for ϕ_2 is

$$\begin{aligned} \delta_{44}\partial^2\phi_2/\partial x_1^2 = & 2[b_1 - R_{11}\sigma_2 - R_{12}(\sigma_1 + \sigma_3) \\ & + b_{12}(\phi_1^2 + \phi_3^2)]\phi_2 - R_{44}(\sigma_6\phi_1 + \sigma_4\phi_3) \end{aligned} \quad (39)$$

with $\sigma_1 = \sigma_6 = 0$, while the equations for ϕ_1 and ϕ_3 are unmodified. This problem is similar to that at the beginning of this section, except that the operator (18) is now replaced by

$$\hat{L} \equiv -\delta_{44}\frac{d^2}{dx_1^2} + C + Uf^2\left(\frac{x_1}{t_w}\right), \quad (40)$$

where $f^2(x)$ is a more complicated expression which, however, has the property to reach its absolute minimum 0 at $x=0$. C is by definition the inverse susceptibility (with respect to ϕ_2) in the middle of the wall, here

$$C = 2(b_1 - R_{11}\sigma_2 - R_{12}\sigma_3 + b_{12}\phi_1^2). \quad (41)$$

The expressions for σ_2 and σ_3 can be calculated as above. As explained at the beginning of this section, a necessary condition for the instability is $C < 0$. Using the ratio $\{\phi_1^2\}_m/\phi_0^2$ given by Eq. (38), together with the definitions (26), this condition can be written

$$1 - \frac{2b_{11}}{b_{12}} < 1 - \frac{\left(1 + \frac{R_{12}}{2b_{11}} \frac{R_{11} + R_{12}}{s_{11} + s_{12}}\right) \left(1 + \frac{R_{12}}{2b_{12}} \frac{R_{11} + R_{12}}{s_{11} + s_{12}}\right)}{\left\{1 + \frac{1}{4b_{11}} \left[\frac{(R_{11} + R_{12})^2}{s_{11} + s_{12}} - \frac{(R_{11} - R_{12})^2}{s_{11} - s_{12}}\right]\right\} \left\{1 + \frac{R_{12}^2}{b_{11}(s_{11} + s_{12})}\right\}}. \quad (42)$$

In the absence of mechanical couplings, the RHS is zero and the condition reduces to $2b_{11}/b_{12} > 1$ which actually corresponds to the instability of the tetragonal phase with respect to the trigonal one.⁵ Hence, in SrTiO₃ one must have $2b_{11}/b_{12} < 1$ and the difference $1 - 2b_{11}/b_{12} = 0.13$ is well known as it can be derived from the splitting of the structural soft modes at low T .⁷ It turns out that the elastic corrections on the RHS of Eq. (42) are far from sufficient to make it bigger than 0.13. A numerical evaluation of the RHS, using the parameters in the Appendix, gives the value 0.04. Evaluating the influence of inaccuracies of 10%, cumulated on all six parameters entering the RHS, we find that the result is then between 0.02 and 0.06. This being so much smaller than 0.13, we conclude that the Néel boundary is extremely likely to be stable against the development of the third component of the structural order parameter.

A final remark concerns the possible existence of a Bloch wall with $\phi_1 = 0$ and $\phi_2 \neq 0$. The simple wall with only $\phi_3 \neq 0$ is indeed unstable both against the spontaneous appearance of ϕ_1 or that of ϕ_2 . However, the eigenvalue associated with the development of ϕ_1 is much more negative than the one for ϕ_2 . This shows that the Néel wall is preferred over the Bloch wall.

IV. FERROELECTRIC INSTABILITY WITHIN ANTIPHASE BOUNDARIES

It is well known that in perovskites there is generally a competition between the development of the structural order parameter and that of ferroelectricity. In strontium titanate, it has been shown that if the structural transition could be suppressed, then under mechanically free conditions the ferroelectricity should occur at ≈ 30 K.¹⁰ For this reason one can expect that under favorable circumstances a ferroelectric transition might occur in an antiphase boundary. To find out under which conditions this actually happens, one must consider three additional factors: (1) the mechanical coupling of the boundary region with the adjacent bulk, (2) the effect of the eventual new components of $\vec{\phi}$ in the wall, (3) the energy associated with the inhomogeneous distribution of the polarization developing in the wall. Such an instability will be sensitive to the orientation of the boundary. In this work we just consider two extreme cases: (a) the longitudinal or “easy” wall and (b) the transverse or “hard” wall with its normal parallel to a $\langle 100 \rangle$ direction of the cubic phase as discussed in Sec. III. We find that in the former case there is no ferroelectric instability whereas in the latter a polarization develops along the \vec{c} axis of the bulk.

To carry out this program, the Gibbs function (1) has to be completed with the terms G_P containing the polarization vector \vec{P} . This part is written

$$\begin{aligned}
G_P = & a_1(P_1^2 + P_2^2 + P_3^2) + a_{11}(P_1^4 + P_2^4 + P_3^4) + a_{12}(P_1^2 P_2^2 + P_2^2 P_3^2 + P_3^2 P_1^2) - Q_{11}(P_1^2 \sigma_1 + P_2^2 \sigma_2 + P_3^2 \sigma_3) \\
& - Q_{12}[(P_2^2 + P_3^2) \sigma_1 + (P_3^2 + P_1^2) \sigma_2 + (P_1^2 + P_2^2) \sigma_3] - Q_{44}(P_2 P_3 \sigma_4 + P_3 P_1 \sigma_5 + P_1 P_2 \sigma_6) - t_{11}(P_1^2 \phi_1^2 + P_2^2 \phi_2^2 + P_3^2 \phi_3^2) \\
& - t_{12}[\phi_1^2(P_2^2 + P_3^2) + \phi_2^2(P_3^2 + P_1^2) + \phi_3^2(P_1^2 + P_2^2)] - t_{44}(P_2 P_3 \phi_2 \phi_3 + P_3 P_1 \phi_1 \phi_3 + P_1 P_2 \phi_1 \phi_2) + \frac{1}{2} \kappa_{11}[(\partial P_1 / \partial x_1)^2 \\
& + (\partial P_2 / \partial x_2)^2 + (\partial P_3 / \partial x_3)^2] + \kappa_{12}[(\partial P_1 / \partial x_1)(\partial P_2 / \partial x_2) + (\partial P_2 / \partial x_2)(\partial P_3 / \partial x_3) + (\partial P_3 / \partial x_3)(\partial P_1 / \partial x_1)] \\
& + \frac{1}{2} \kappa_{44}[(\partial P_1 / \partial x_2 + \partial P_2 / \partial x_1)^2 + (\partial P_2 / \partial x_3 + \partial P_3 / \partial x_2)^2 + (\partial P_3 / \partial x_1 + \partial P_1 / \partial x_3)^2] \\
& + f_{11} \left[\frac{\partial P_1}{\partial x_1} \sigma_1 + \frac{\partial P_2}{\partial x_2} \sigma_2 + \frac{\partial P_3}{\partial x_3} \sigma_3 \right] + f_{12} \left[\left(\frac{\partial P_1}{\partial x_1} + \frac{\partial P_2}{\partial x_2} \right) \sigma_3 + \left(\frac{\partial P_2}{\partial x_2} + \frac{\partial P_3}{\partial x_3} \right) \sigma_1 + \left(\frac{\partial P_3}{\partial x_3} + \frac{\partial P_1}{\partial x_1} \right) \sigma_2 \right] \\
& + f_{44} \left[\left(\frac{\partial P_1}{\partial x_2} + \frac{\partial P_2}{\partial x_1} \right) \sigma_6 + \left(\frac{\partial P_2}{\partial x_3} + \frac{\partial P_3}{\partial x_2} \right) \sigma_4 + \left(\frac{\partial P_3}{\partial x_1} + \frac{\partial P_1}{\partial x_3} \right) \sigma_5 \right]. \tag{43}
\end{aligned}$$

In addition to the usual gradient terms with coefficients κ_{ij} , we have included the flexoelastic terms in f_{ij} which do have an appreciable renormalization effect on κ as explained in the Appendix. The Appendix also gives the values of the necessary coefficients.

A. Local instability

As a first step, one can check whether ferroelectricity can occur in the middle of the boundary neglecting the gradient contributions to the energy. We call the corresponding instability a ‘‘local’’ polarization instability. Physically, this amounts to considering the hypothetical situation of a polarization instability in an infinitely thick boundary. This is a necessary condition to obtain the instability in a real boundary. To check for the local polarization instability, it is sufficient to calculate the inverse susceptibility $\partial^2 G_P / \partial P_i^2$ for the relevant component P_i . In general, the polarization component perpendicular to the boundary will not be able to develop because of the depolarizing effects, and thus the relevant components of P_i lie in the boundary plane.

We take as first example the longitudinal boundary perpendicular to the x_3 axis that was discussed in connection with Eqs. (15) and (16). The relevant polarization components are P_1 and P_2 , but in view of the symmetry of the problem it suffices to check for P_1 . The corresponding inverse susceptibility is given by

$$\chi_1^{-1} = \frac{\partial^2 G_P}{\partial P_1^2} = 2(a_1 - Q_{11} \sigma_1 - Q_{12} \sigma_2 - t_{12} \phi_3^2), \tag{44}$$

where

$$\sigma_1 = \sigma_2 = R_{12} \frac{\phi_0^2 - \phi_3^2}{s_{11} + s_{12}}. \tag{45}$$

In the center of the wall $\phi_3 = 0$ and

$$\{\chi_1^{-1}\}_m = 2 \left[a_1 - (Q_{11} + Q_{12}) R_{12} \frac{\phi_0^2}{s_{11} + s_{12}} \right], \tag{46}$$

where ϕ_0 is the bulk value of ϕ_3 given by Eq. (7). Using the known value of the bare inverse susceptibility $2a_1$ (Appendix), the T dependence of the corresponding dielectric constant $\epsilon_{1,2}^l = 4\pi \{\chi_1\}_m$ shown in Fig. 3 is obtained. It does not diverge, and thus the longitudinal antiphase boundary is stable against the development of a spontaneous polarization.

As a second example we take the transverse boundary perpendicular to the x_1 direction calculated in the previous section. In this case one must check separately for P_2 and P_3 . For P_2 one obtains

$$\{\chi_2^{-1}\}_m = 2[a_1 - Q_{11}\{\sigma_2\}_m - Q_{12}\{\sigma_3\}_m - t_{12}\{\phi_1^2\}_m], \tag{47}$$

where all values are in the middle of the boundary. $\{\sigma_{2,3}\}_m$ can be obtained from Eq. (13), with extra terms owing to the fact that now $\phi_1 \neq 0$. One finds

$$\begin{aligned}
\{\sigma_2\}_m &= \frac{s_{11} R_{12} - s_{12} R_{11}}{s_{11}^2 - s_{12}^2} \phi_0^2 - \frac{R_{12}}{s_{11} + s_{12}} \{\phi_1^2\}_m, \\
\{\sigma_3\}_m &= \frac{s_{11} R_{11} - s_{12} R_{12}}{s_{11}^2 - s_{12}^2} \phi_0^2 - \frac{R_{12}}{s_{11} + s_{12}} \{\phi_1^2\}_m. \tag{48}
\end{aligned}$$

Inserting these into Eq. (47), and using $\{\phi_1^2\}_m$ from Eq. (38), the numerical result for the local dielectric constant $\epsilon_2^l = 4\pi \{\chi_2\}_m$ shown in Fig. 3 is obtained. This transverse boundary is thus stable against the spontaneous development of P_2 .

Finally, let us consider the case of P_3 . One finds

$$\begin{aligned}
 \{\chi_3^{-1}\}_m &= 2[a_1 - Q_{11}\{\sigma_3\}_m - Q_{12}\{\sigma_2\}_m - t_{12}\{\phi_1^2\}_m] \\
 &= 2\left[a_1 - \left(Q_{11} \frac{s_{11}R_{11} - s_{12}R_{12}}{s_{11}^2 - s_{12}^2} \right. \right. \\
 &\quad \left. \left. + Q_{12} \frac{s_{11}R_{12} - s_{12}R_{11}}{s_{11}^2 - s_{12}^2} \right) \phi_0^2 \right] \\
 &\quad + 2\left(R_{12} \frac{Q_{11} + Q_{12}}{s_{11} + s_{12}} - t_{12} \right) \{\phi_1^2\}_m. \quad (49)
 \end{aligned}$$

Inserting the values as above, the numerical result for $\epsilon_3^t = 4\pi\{\chi_3\}_m$ shown in Fig. 3 is found. This now reveals a local instability at ≈ 42 K. Therefore this boundary is a candidate for a true ferroelectric instability which should now be checked making allowance for the effects of the boundary profile and of the polarization-gradient energy.

Before doing this, it is of interest to consider the physical origin of the deviations of the ‘‘local’’ dielectric constants shown in Fig. 3 from their bulk values. The deviations from the bare susceptibility can be discussed in terms of separate contributions from pure strains and from pure rotations, as done for the bulk in Ref. 10.

(i) In the bulk, as shown in Ref. 10, while the bare dielectric susceptibility diverges around 30 K, this divergence is prevented in the case of ϵ_a mostly by the stabilizing effect of the phase-transition-induced compressive strains in the ab plane. In the case of ϵ_c , there are several contributions but the one which is by far dominant is the strong stabilizing effect of the pure ϕ_3 rotation around the \vec{c} axis.

(ii) For the ‘‘easy’’ antiphase boundary, the strains in the ab plane are just like those in the bulk, and thus the polarization instability in the boundary is suppressed mostly for the same reason. There are of course differences between ϵ_a and $\epsilon_{1,2}^t$ which arise from the lesser contributions.

(iii) For the ‘‘hard’’ boundary perpendicular to x_1 , the adjacent bulk produces a compressive strain ϵ_2 and an elongation ϵ_3 . It is principally ϵ_2 that prevents the P_2 instability, just as it does in the bulk. On the other hand ϕ_3 is zero in the middle of the boundary, and this removes the main stabilizing effect on P_3 . One is essentially back to the situation of the cubic phase, because the effect of ϕ_1 is minor. Owing to the imposed elongation along x_3 , the instability of P_3 is then enhanced, which raises the expected transition temperature from ~ 30 to ~ 40 K.

B. Dielectric instability of the Néel wall

Now we investigate in detail the P_3 -instability of the Néel wall whose profile was obtained in Sec. III. This requires the linearized equation of state for P_3 which is calculated from

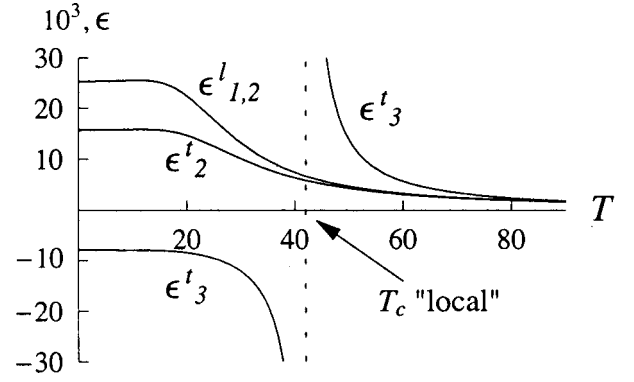


FIG. 3. The local dielectric constants calculated in the middle of a longitudinal wall $\epsilon_{1,2}^l$, and in the middle of a transverse wall perpendicular to the x_1 axis, ϵ_2^t and ϵ_3^t . The values found for $\epsilon_{1,2}^l$ and ϵ_2^t are smaller than ϵ_a in the bulk, whereas the value of ϵ_3^t is much larger than the corresponding ϵ_c of the bulk, and it diverges at 42 K.

$$\frac{\partial}{\partial x_1} [\partial G_P / \partial (\partial P_3 / \partial x_1)] = \partial G_P / \partial P_3 \quad (50)$$

and Eq. (43). Note that in this case the RHS of Eq. (50) is simply $[\partial^2 G_P / \partial P_3^2] P_3$. This second derivative can be written

$$\frac{\partial^2 G_P}{\partial P_3^2} = C + U\Theta(x_1/t_w), \quad (51)$$

where $\Theta(x_1/t_w)$ is zero at the center of the wall $x_1 = 0$ and is 1 on its exterior $x_1 \rightarrow \pm\infty$. With this notation the equation of state reduces to

$$-\kappa_{44} \partial^2 P_3 / \partial x_1^2 + [C + U\Theta(x_1/t_w)] P_3 = 0, \quad (52)$$

where C is obviously the inverse susceptibility in the center of the wall given by Eq. (49), while

$$C + U = \left(\frac{\partial^2 G_P}{\partial P_3^2} \right)_{\pm\infty} = 2(a_1 - t_{11}\phi_0^2). \quad (53)$$

The linear operator of interest here is thus

$$\hat{L} = -\kappa_{44} \frac{d^2}{dx_1^2} + C + U\Theta(x_1/t_w). \quad (54)$$

It remains to obtain the expression for $\Theta(x_1/t_w)$. A direct calculation gives

$$\Theta = \frac{Q_{11}[\{\sigma_3\}_m - \sigma_3] + Q_{12}[\{\sigma_2\}_m - \sigma_2] + t_{12}[\{\phi_1^2\}_m - \phi_1^2] - t_{11}\phi_3^2}{Q_{11}\{\sigma_3\}_m + Q_{12}\{\sigma_2\}_m + t_{12}\{\phi_1^2\}_m - t_{11}\phi_0^2}, \quad (55)$$

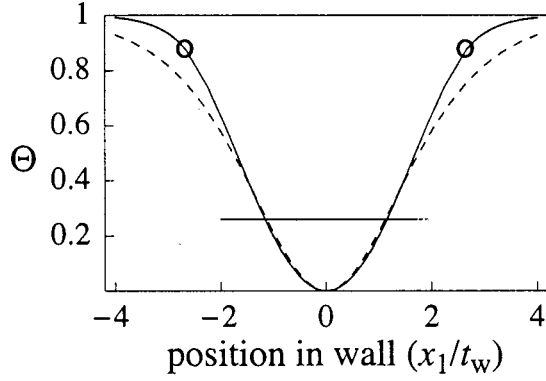


FIG. 4. The function $\Theta(x_1/t_w)$ given by Eq. (55), which enters the eigenvalue equation that determines the dielectric instability of a hard Néel-type boundary. The open dots show the crossover points between the two branches. The approximation of Θ with $\tanh^2(x_1/t_N)$ is shown by the dashed line. The horizontal bar is the actual lowest eigenvalue before the addition of $-|C|$ in Eq. (54). It shows that Θ is particularly well approximated in that region.

where

$$\begin{aligned} \{\sigma_2\}_m - \sigma_2 &= \frac{s_{11}R_{12} - s_{12}R_{11}}{s_{11}^2 - s_{12}^2} \phi_3^2 - \frac{R_{12}}{s_{11} + s_{12}} [\{\phi_1^2\}_m - \phi_1^2], \\ \{\sigma_3\}_m - \sigma_3 &= \frac{s_{11}R_{11} - s_{12}R_{12}}{s_{11}^2 - s_{12}^2} \phi_3^2 - \frac{R_{12}}{s_{11} + s_{12}} [\{\phi_1^2\}_m - \phi_1^2]. \end{aligned} \quad (56)$$

It is obvious that Eq. (55) has the property $\{\Theta\}_m = 0$ since $\{\phi_3^2\}_m = 0$, and $\{\Theta\}_{\pm\infty} = 1$ since $\sigma_3 = \sigma_2 = 0$ in the bulk. The calculated curve $\Theta(x_1/t_w)$ is shown in Fig. 4. It can be approximated quite satisfactorily by $\tanh^2(x_1/t_N)$, where the approximate half-width of the Néel boundary is $t_N \approx 2t_w$. This approximation is shown by the dashed line in Fig. 4. The position of the first eigenvalue shown by the horizontal line is sufficiently deep in the well that it should not be substantially affected by the quality of the approximation in the wings. With this the problem is identical to that treated with the operator (18). The condition for instability is just given by the equivalent of Eq. (21):

$$U + C < C^2 t_N^2 / \kappa_{44}. \quad (57)$$

Here the LHS is given by Eq. (53) and it is just $4\pi/\epsilon_c$. This quantity is plotted in Fig. 5, as derived from the soft-mode frequency measurement (Appendix). The RHS contains C as given by Eq. (49). Our best value of the RHS is shown by the corresponding solid line in this figure. It intercepts $4\pi/\epsilon_c$ at $T_c \approx 39$ K. The dashed lines illustrate that a $\pm 30\%$ multiplicative inaccuracy in the RHS introduces at most a 1 K inaccuracy in T_c . However, the main inaccuracy is hidden in the exact value of the bare inverse susceptibility $2a_1$, and more precisely in the position of its zero around 30 K. A shift of that point results in a shift of the 42 K zero on the RHS of Eq. (57), and in a horizontal shift of the corresponding curves in Fig. 5. In consequence, a reasonable estimate for

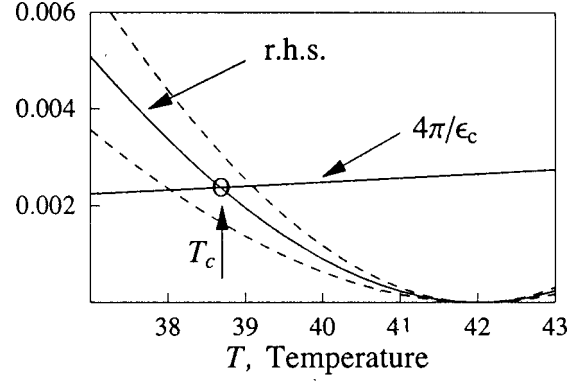


FIG. 5. Determination of T_c following Eq. (57). The line $4\pi/\epsilon_c$ is the LHS of Eq. (57). It intercepts the RHS at the transition temperature T_c . The dashed lines indicate the small effect on T_c of a $\pm 30\%$ variation of the numerical values on the RHS. The main uncertainty comes, in fact, from the position of the zero of the “local” inverse susceptibility C .

the value of T_c might be between 35 and 40 K. It should be remarked that the effects of the boundary profile and of the polarization-gradient terms are rather small. They reduce the “local” value of T_c by only ~ 3 K, i.e., by less than 10%. The boundary being rather thick, the situation is in fact close to that of a transition in bulk material, but with the “local” instability temperature.

C. The saturation polarization

It is of interest to obtain an estimate for the size of the polarization that develops below T_c . We assume for that calculation that the boundary experiences no further instability below T_c , and we simply determine the saturation value at 0 K which is set by the quartic term a_{11} in G_P , Eq. (43). For such an estimate it is also reasonable to just use a “local” Gibbs potential in the middle of the boundary, as we have shown in the previous subsection that the modifications due to the profile are comparatively small. The relevant part of G_P is then

$$\{G\}_m = \frac{1}{2} \{\chi_3^{-1}\}_m P_3^2 + a_{11} P_3^4 + Q_{11} \sigma_3' P_3^2 + Q_{12} \sigma_2' P_3^2. \quad (58)$$

The value of $\{\chi_3^{-1}\}_m$ is given by Eq. (49). The primed stresses σ_2' and σ_3' are just the P_3^2 -induced changes in σ_2 and σ_3 , as the main part of the stresses is already included in the calculation of $\{\chi_3^{-1}\}_m$. The induced changes in ϕ_1 and ϕ_3 are neglected in this simple estimate, as it can be shown that their effect is comparatively quite small. Since the macroscopic field is zero, $E = \partial\{G\}_m/\partial P_3 = 0$, the derivative in P_3 of Eq. (58) gives an equation for the saturation polarization P_s . The values of σ_2' and σ_3' that enter that equation are obtained from Eq. (3):

$$\begin{aligned} \delta\epsilon_2 &= s_{11}\sigma_2' + s_{12}\sigma_3' - Q_{12}P_s^2, \\ \delta\epsilon_3 &= s_{12}\sigma_2' + s_{11}\sigma_3' - Q_{11}P_s^2. \end{aligned} \quad (59)$$

As the strains are fixed by the adjacent domains, the changes $\delta\varepsilon_2$ and $\delta\varepsilon_3$ are zero, so that Eq. (59) gives

$$\begin{aligned}\sigma'_2 &= \frac{Q_{12}^s s_{11} - Q_{11}^s s_{12}}{s_{11}^2 - s_{12}^2} P_s^2, \\ \sigma'_3 &= \frac{Q_{11}^s s_{11} - Q_{12}^s s_{12}}{s_{11}^2 - s_{12}^2} P_s^2.\end{aligned}\quad (60)$$

Introducing these in the derivative of Eq. (58), one finds that a_{11} is renormalized to

$$\tilde{a}_{11} = a_{11} + \frac{(Q_{11}^2 + Q_{12}^2)s_{11} - 2Q_{11}Q_{12}s_{12}}{2(s_{11}^2 - s_{12}^2)}.\quad (61)$$

Finally, P_s is given by

$$P_s^2 = -\frac{\{\chi_3^{-1}\}_m}{4\tilde{a}_{11}},\quad (62)$$

where $\{\chi_3^{-1}\}_m$ is at 0 K. Introducing the numerical values from the Appendix, one finds $P_s^2 = 1.9 \times 10^8$ cgs, or $P_s = 4.2 \mu\text{C}/\text{cm}^2$. This is quite a large value, as it amounts to about 20% of the room-temperature polarization of a strong ferroelectric such as BaTiO_3 . The corresponding stresses $\sigma'_2 = -0.16 \times 10^8$ and $\sigma'_3 = 2.7 \times 10^8$ erg/cm³ are also quite large.

V. DISCUSSION

The solutions for “simple” antiphase boundaries were presented in Sec. II and the stability of these solutions against the development of other components of $\vec{\phi}$ was analyzed in Sec. III. The “simple” boundary, with $\phi = 0$ in its middle, is the stable solution when its plane is perpendicular to the tetragonal axis \vec{c} . These we also called longitudinal, or “easy” boundaries. They are quite thin since the continuum approximation only gives a full width $2t_w \approx 2a_0$. This means that a microscopic calculation will be necessary to establish their structure. Such boundaries have been observed with high-resolution electron microscopy.²⁸ On the very thin samples used in such a case, they were indeed found to be rather sharp, and also to have an extremely high density, different boundaries being separated from each other by just a few times a_0 .

It was also shown in Sec. III that “simple” transverse boundaries, those that contain the \vec{c} axis, are unstable against the development of new components of $\vec{\phi}$. This is found for all values of the angle α between the normal to the boundary and the x_1 direction. For the particular case $\alpha = 0$, the stable structure was shown to be of the Néel type. For these particular orientations an analytical solution could be obtained by neglecting δ_{11} . That approximation is physically well justified, in view of the nearly two-dimensional (2D) correlation of the TiO_6 -octahedra rotations in the basal plane. These Néel boundaries are very thick, with a full width $2t_N \approx 20$ to $25a_0$. This justifies the use of the continuous approximation.

These boundaries can also be called “hard” in view of their higher energy compared to the “easy” ones.

In Sec. IV, it was shown that the $\alpha = 0$ hard boundary is unstable with respect to the development of a spontaneous polarization parallel to \vec{c} . This unusual ferroelectric transition should occur for T_c between ~ 35 and ~ 40 K. The question naturally arises whether this is a general feature of all the hard boundaries, irrespective of α . A strict answer to this question would require solutions for the Néel-type boundaries at all α 's, including checking for their stability. For $\alpha \neq 0$ the approximation $\delta_{11} = 0$ is of no particular advantage, so that one is faced with having to solve a pair of coupled nonlinear differential equations. This is generally quite a tedious task that should require a numerical study, as it seems that it cannot be pursued analytically.^{26,18} However, we found for $\alpha = 0$ that the ferroelectric instability was neither strongly affected by the gradient terms, nor by the presence of the component of $\vec{\phi}$ perpendicular to the boundary plane. It is thus meaningful to check for the “local” polarization instability in the middle of “simple” hard boundaries, even though these are structurally unstable. We found in that approximation very similar P_3 instabilities for $\alpha = 0$ and for $\alpha = \pi/4$, with nearly equal values of T_c . This leads us to conjecture that ferroelectric instabilities should occur in hard boundaries for all values of α , and in all at about the same T_c . The above result for $\alpha = 0$, and conjecture for all α 's, might provide an explanation for some of the numerous unexplained anomalies that have been reported in SrTiO_3 between ~ 30 and ~ 40 K.

In a first extensive x-ray study, Lytle already reported a transition-like feature occurring at ~ 35 K.²⁹ In retrospect, what he observed might have been a rearrangement of *structural* domains, i.e., essentially an exchange of a for c or vice versa within the scattering volume. Such structural anomalies are of course numerous, and they have a clear signature in ultrasonic measurements, as well as in mechanical or electromechanical ones, such as, e.g., in Refs. 30 or 31. It is important not to mistake these effects for genuine “bulk” ones. Take for example the case of an ultrasonic measurement of a shear velocity related to the compliance s_{44} of the cubic phase. If nothing is undertaken to generate a “single tetragonal domain,” the measurement in the tetragonal phase will be affected in an uncontrolled manner by combinations of the *tetragonal* compliances s_{44} and s_{66} , which are quite different from each other.⁵ A complicated behavior is then seen in the tetragonal phase, as, e.g., in Ref. 32. By application of a sufficient orienting $\langle 110 \rangle$ -axial pressure, such anomalies can be forced to disappear from the ultrasonic data.¹³ It is, however quite interesting that anomalies related to domain motion, similar to the one just cited or the mechanical friction peak reported in Ref. 31, occur in the region of the T_c predicted above. This suggests that the ferroelectric transition in the antiphase boundaries can modify substantially the mobility of the structural domains. This is probably not so surprising considering the interaction between ferroelastic boundaries and antiphase ones that is known in materials such as gadolinium molybdate (GMO).^{33,34}

There are also reports of “bulk” anomalies in the same T

region. This is the case for the effects at T_q , originally noticed with electron paramagnetic resonance (EPR),¹² but also seen on other signatures such as birefringence.^{35,11} EPR measurements were often performed on thin, elongated, highly polished platelets that had been cut with a specific crystalline orientation.³⁶ These platelets have the nice property to transform with a single tetragonal-axis direction below T_a . One may presume that a large number of dislocations become oriented plastically during polishing, producing the internal stresses that force the “monodomain” character. The birefringence measurement of Ref. 35 also used such a sample. The “Müller effect”¹² was observed on elongated, polished, thin rods which might have quite similar structural defects. In all these “real” samples, the density and orientation of antiphase boundaries will not be determined by thermodynamic equilibrium, but rather by defects and transition-kinetic considerations. In thin polished samples one should expect a large density of antiphase boundaries that form and “freeze in” owing to edge dislocations. A link between antiphase boundaries and dislocations was experimentally observed in GMO.^{33,34} If the density of hard boundaries is sufficiently high, the stresses generated within the boundaries by the ferroelectric transition will have to be equilibrated by additional average strains that will affect the entire sample. The onset of these strains at T_c might well produce transition-like features near T_q in bulk measurements. This would of course explain why strong effects at T_q are not seen in thick, good quality samples that are forced into a single tetragonal orientation by an external axial pressure, as in Refs. 37 and 10.

The ferroelectricity which we predict in “hard” antiphase boundaries below 40 K should also manifest itself in dielectric losses. The loss can be influenced over a wide frequency range. Slabs of polar material, i.e., ferroelectric antiphase boundaries, will affect the loss mainly owing to two effects. Firstly, the so-called quasi-Debye loss mechanism (see e.g., Ref. 38) allowed by symmetry only in noncentrosymmetric structures will be active in these boundaries. The contribution of this mechanism can be essential at microwave frequencies. Although affecting only a small fraction of the volume, this contribution can really be significant as its yield is expected to be very large per unit volume.^{39,40} Secondly, the ferroelectric slabs should split into ferroelectric subdomains divided by subdomain walls—the regions where the spontaneous polarization passes through zero. These subdomains will contribute to the dielectric loss as the domain walls in bulk ferroelectrics do. This contribution could be relevant at lower frequencies, similar to the case of bulk ferroelectrics. We believe these mechanisms could be relevant to the observed low temperature anomalies in the dielectric losses of SrTiO₃ as reported for microwaves in Ref. 14 and for radio frequencies in Ref. 15. Clearly, a direct test for this interpretation will require experiments where the type and amount of antiphase boundaries will also be monitored.

In conclusion, the predicted ferroelectric transition within antiphase boundaries can potentially produce a large number of anomalies as it occurs. Further progress along this line will require the development of experimental methods to produce, observe, and control these boundaries. More gener-

ally, it should be remarked that a “local” ferroelectric instability is clearly possible in SrTiO₃ when the antiferrodistortive order parameter is locally modified, especially if the strains are favorable. One should thus keep in mind that other structural defects than “hard” boundaries could possibly generate a local transition, and thereby anomalies, in the same temperature region.

VI. SUMMARY

We have shown in this paper that the antiphase domain boundaries that occur below the 105 K structural phase transition of SrTiO₃ are of two extreme types. Boundaries perpendicular to the tetragonal axis are very thin and characterized by a single component of the structural order parameter, as already discussed previously.¹⁸ Boundaries containing the tetragonal axis are much thicker ($\sim 20a_0$) and an additional component of the order parameter develops within them, so that they are of the Néel type. Near or below 40 K, a ferroelectric transition should occur in these boundaries. The developed polarization is sizable as it could reach values $\sim 4 \mu\text{C}/\text{cm}^2$. The discussion in Sec. V suggests that such a transition could possibly account for several of the so far unexplained anomalies which have been reported for SrTiO₃ below ~ 40 K.

ACKNOWLEDGMENTS

The authors thank B. Hehlen for communicating unpublished experimental data that have been inspiring. A.K.T. has benefitted from the hospitality of the Laboratoire des Verres and the CNRS in Montpellier, where a large part of this research was done. He also acknowledges the financial support of the Swiss National Foundation.

APPENDIX

This appendix lists all the numerical values that are used in the course of the paper. The only temperature dependent parameters are b_1 in Eq. (1) and a_1 in Eq. (43). All other parameters are assumed constant and the values that have been used are listed in Table I. The sources are indicated in the caption of the table. The calculations that were performed to obtain some of these coefficients are straightforward, with the exception of those for κ_{44} and f_{44} which will now be explained.

A value of κ_{44} can be derived from the dispersion with wave vector \vec{q} of the ferroelectric transverse optic (TO) soft mode. This has been determined with neutron scattering.^{37,44} The value $\tilde{\kappa}_{44}$ which is obtained in this way is, however, renormalized by the coupling between the gradient of the polarization and the transverse acoustic waves.^{45,46} This coupling is produced by the flexoelectric tensor f . To understand the situation it is easiest to first derive the coupled equations of motion from the Gibbs function used here. The equation for the polarization P_3 of the TO mode propagating in the x_1 direction is

TABLE I. Constants of ‘‘cubic’’ SrTiO₃ at low temperatures.

b_{11}	1.69×10^{43} a	a_{11}	2.1×10^{-12} f
b_{12}	3.88×10^{43} a	a_{12}	1.7×10^{-12} f
s_{11}	3.52×10^{-13} b	Q_{11}	5.09×10^{-13} g
s_{12}	-0.85×10^{-13} b	Q_{12}	-1.50×10^{-13} g
s_{44}	7.87×10^{-13} b	Q_{44}	2.13×10^{-13} g
R_{11}	8.7×10^{14} c	t_{11}	-1.94×10^{15} h
R_{12}	-7.8×10^{14} c	t_{12}	-0.84×10^{15} h
R_{44}	-18.4×10^{14} c	t_{44}	6.51×10^{15} h
δ_{11}	0.28×10^{11} d	κ_{11}	not used
δ_{12}	-7.34×10^{11} d	κ_{12}	not used
δ_{44}	7.11×10^{11} d	κ_{44}	8.26×10^{-18} i
ρ	5.13 b	f_{11}	not used
a_0	3.9×10^{-8} b	f_{12}	not used
$\Lambda/4\pi$	7.24×10^{27} e	f_{44}	5.88×10^{-15} i

^aRecalculated from constant-strain values in Ref. 7.

^bFrom Ref. 41.

^cFrom Ref. 7.

^dFrom Ref. 18 corrected according to the units used in the original paper by Stirling (Ref. 16).

^e $\Lambda \equiv \epsilon_{a,c} \Omega_{a,c}^2$ where $\Omega_{a,c}$ is the soft-mode frequency in rad/s. The value is calculated from the data in Ref. 10 taking $(\epsilon_a)_{\max} = 42000$ and $(\epsilon_c)_{\max} = 9400$.

^fRecalculated from constant-strain values in Ref. 42.

^gRecalculated from the deformation-polarization electrostrictive coefficients in Ref. 43.

^hRecalculated from data in Ref. 10, keeping $t_{11} - t_{12}$ at the value of Ref. 7. The difference with Ref. 10 is due to a numerical error in the latter.

ⁱExplained in the Appendix.

$$\gamma \ddot{P}_3 + \partial G_P / \partial P_3 = \frac{d}{dx_1} [\partial G_P / \partial (\partial P_3 / \partial x_1)], \quad (\text{A1})$$

which gives

$$\gamma \ddot{P}_3 + 2a_1 = \kappa_{44} \frac{d^2 P_3}{dx_1^2} + f_{44} \frac{d\sigma_5}{dx_1}. \quad (\text{A2})$$

The equation for σ_5 is obtained from the constitutive equations of elasticity (3) with $G = G_\phi + G_P$. Taking into account Eqs. (1) and (43), it reads

$$\varepsilon_5 = s_{44} \sigma_5 - f_{44} \frac{dP_3}{dx_1}. \quad (\text{A3})$$

Introducing this into Eq. (A2) and using $d\varepsilon_5/dx_1 = d^2 u_3 / dx_1^2$, where u_3 is a component of the acoustical displacement, one obtains

$$-\gamma \ddot{P}_3 = \left[2a_1 - \left(\kappa_{44} + \frac{f_{44}^2}{s_{44}} \right) \frac{d^2}{dx_1^2} \right] P_3 - \frac{f_{44}}{s_{44}} \frac{d^2 u_3}{dx_1^2}. \quad (\text{A4})$$

This exhibits the coupling between P_3 and u_3 . The equation of motion for u_3 , including the flexoelectric term, reads

$$-\rho \ddot{u}_3 = \frac{1}{s_{44}} \frac{d^2 u_3}{dx_1^2} + \frac{f_{44}}{s_{44}} \frac{d^2 P_3}{dx_1^2}, \quad (\text{A5})$$

where ρ is the density of the crystal. Now one introduces the displacement P for the TO-mode by $P_3 \equiv \sqrt{\rho/\gamma} P$, and transforms to Fourier space with $P \propto u_3 \propto \exp(-i\omega t + iq x_1)$. One obtains

$$\begin{aligned} \omega^2 P &= \Omega_{TO}^2 P + V q^2 u_3, \\ \omega^2 u_3 &= V q^2 P + \Omega_{TA}^2 u_3, \end{aligned} \quad (\text{A6})$$

where

$$\begin{aligned} \Omega_{TO}^2 &= (2a_1 + \tilde{\kappa}_{44} q^2) / \gamma, \\ \Omega_{TA}^2 &= q^2 / (\rho s_{44}), \\ \tilde{\kappa} &= \kappa + f_{44}^2 / s_{44}, \\ V &= f_{44} / (s_{44} \sqrt{\rho \gamma}). \end{aligned} \quad (\text{A7})$$

It is clear from the first relation, since $2a_1 = 4\pi/\epsilon$, that $\gamma = 4\pi/\Lambda$, where Λ is defined in Table I. The neutron scattering experiments^{37,44} determine $\tilde{\kappa}_{44}/\gamma = 3.8 \times 10^{11}$ cm²/s². The value of V was found by Brillouin scattering experiments⁴⁶ $V = 2.4 \times 10^{11}$ cm²/s². The same experiments give the bare velocity $\Omega_{TA}/q = 4.25 \times 10^5$ cm/s. From these values, using (A7), one calculates $\tilde{\kappa}_{44} = 5.23 \times 10^{-17}$ cm² and $\kappa_{44} = 0.826 \times 10^{-17}$ cm². This emphasizes the large effect of the flexoelectric renormalization.

The value of b_1 in Eq. (1) is only used here in the low- T phase, well below $T_a = 105$ K. It is related to ϕ_0^2 by Eq. (7). The experimental value of ϕ_0^2 was taken from Ref. 47 and converted to the units cm² (oxygen displacements as in Ref. 7). It was then fitted to a polynomial function that gives an excellent approximation for $T \leq 60$ K. The result is

$$\begin{aligned} -b_1(T) &= 1.62 \times 10^{25} \\ &\times (1 - 0.338 \times 10^{-4} T^2 - 0.53 \times 10^{-6} T^3). \end{aligned} \quad (\text{A8})$$

The value of a_1 in Eq. (43) is obtained from the measured soft-mode frequencies in Ref. 10, using the value of Λ in Table I. It is already fitted to a Barrett formula in Ref. 10, which in the appropriate cgs units reads

$$a_1(T) = 4.51 \times [\coth(54/T) - \coth(54/30)] \times 10^{-3}. \quad (\text{A9})$$

- ¹M.E. Lines and A.M. Glass, *Principles and Applications of Ferroelectrics and Related Materials* (Oxford University Press, Oxford, 1977).
- ²H.A. Megaw, Proc. Phys. Soc. London **58**, 133 (1946).
- ³H. Unoki and T. Sakudo, J. Phys. Soc. Jpn. **23**, 546 (1967).
- ⁴K.A. Müller, W. Berlinger, and F. Waldner, Phys. Rev. Lett. **21**, 814 (1968).
- ⁵J.C. Slonczewski and H. Thomas, Phys. Rev. B **1**, 3599 (1970).
- ⁶T. Sakudo and H. Unoki, Phys. Rev. Lett. **26**, 851 (1971).
- ⁷H. Uwe and T. Sakudo, Phys. Rev. B **13**, 271 (1976).
- ⁸K.A. Müller and H. Burkard, Phys. Rev. B **19**, 3593 (1979).
- ⁹W. Zhong and D. Vanderbilt, Phys. Rev. Lett. **74**, 2587 (1995).
- ¹⁰A. Yamanaka, M. Kataoka, Y. Inaba, K. Inoue, B. Hehlen, and E. Courtens, Europhys. Lett. **50**, 688 (2000).
- ¹¹E. Courtens, Ferroelectrics **183**, 25 (1996).
- ¹²K.A. Müller, W. Berlinger, and E. Tosatti, Z. Phys. B **84**, 277 (1991).
- ¹³L. Arzel, B. Hehlen, R. Currat, B. Hennion, M. Saint-Paul, and E. Courtens, Ferroelectrics **236**, 81 (2000).
- ¹⁴O.G. Vendik, E.K. Hollman, A.B. Kosyrev, and A.M. Prudan, J. Supercond. **12**, 325 (1999).
- ¹⁵C. Ang, A.S. Balla, R. Guo, and L.E. Cross, Appl. Phys. Lett. **76**, 1929 (2000).
- ¹⁶W.G. Stirling, J. Phys. C **5**, 2711 (1972).
- ¹⁷W.G. Stirling and R. Currat, J. Phys. C **9**, L519 (1976).
- ¹⁸Wenwu Cao and G.R. Barsch, Phys. Rev. B **41**, 4334 (1990).
- ¹⁹V.A. Zhirnov, Zh. Éksp. Theor. Fiz. **35**, 1175 (1958) [Sov. Phys. JETP **35**, 822 (1959)].
- ²⁰The usual definition, $\sigma_{ij} = \sigma_k$ is used, with $k = i$ if $i = j$ and $k = 9 - i - j$ if $i \neq j$.
- ²¹These conditions can be written in the compact form $e_{ijk} e_{plm} [\partial \varepsilon_{jl} / \partial x_k \partial x_m] = 0$, where e_{ijk} is the fully antisymmetric pseudotensor and the usual convention $\varepsilon_k = 2\varepsilon_{ij}$ is used for the off-diagonal strain components. See, e.g., E.A.H. Love, *A Treatise on the Mathematical Theory of Elasticity* (Dove, New York, 1944), p. 49.
- ²²L.N. Bulaevskii and B.G. Vekhter, Zh. Éksp. Theor. Fiz. **91**, 1444 (1986) [Sov. Phys. JETP **64**, 851 (1986)].
- ²³E.B. Sonin and A.K. Tagantsev, Zh. Éksp. Theor. Fiz. **94**, 315 (1987) [Sov. Phys. JETP **67**, 396 (1988)].
- ²⁴J. Lajzerowicz and J.J. Niez, in *Solitons and Condensed Matter Physics*, edited by A.R. Bishop and T. Schneider (Springer Series in Solid-State Sciences, Vol. 8) (Springer Verlag, Berlin, 1981), p. 195.
- ²⁵L.D. Landau and E.M. Lifshitz, *Quantum Mechanics, Vol. 3 of Course of Theoretical Physics* (Pergamon, Oxford, 1958), Sec. 21.
- ²⁶L.N. Bulaevskii and V.L. Ginzburg, Sov. Phys. JETP **18**, 530 (1964).
- ²⁷J. Fousek and V. Janovec, J. Appl. Phys. **40**, 135 (1969).
- ²⁸R. Wang, Y. Zhu, and S.M. Shapiro, Phys. Rev. B **61**, 8814 (2000).
- ²⁹F.W. Lytle, J. Appl. Phys. **35**, 2212 (1964).
- ³⁰G. Sorge, E. Hegenbarth, and G. Schmidt, Phys. Status Solidi **37**, 599 (1970).
- ³¹A. Binder and K. Knorr, Phys. Rev. B **63**, 094106 (2001).
- ³²J.F. Scott and H. Ledbetter, Z. Phys. B: Condens. Matter **104**, 635 (1997).
- ³³V.A. Meleshina, V.L. Indenbom, Kh.S. Bagdasarov, and T.M. Polkhovskaya, Sov. Phys. Crystallogr. **18**, 764 (1974).
- ³⁴V. Janovec, Ferroelectrics **35**, 105 (1981).
- ³⁵E. Courtens, Phys. Rev. Lett. **29**, 1380 (1972).
- ³⁶K.A. Müller, W. Berlinger, M. Capizzi, and H. Gränicher, Solid State Commun. **8**, 549 (1970).
- ³⁷E. Courtens, G. Coddens, B. Hennion, B. Hehlen, J. Pelous, and R. Vacher, Phys. Scr. **T49**, 430 (1993).
- ³⁸V.L. Gurevich and A.K. Tagantsev, Adv. Phys. **40**, 719 (1991).
- ³⁹The contribution of the quasi-Debye mechanism was recently evaluated for KTaO_3 under a dc-bias field (Ref. 40). That calculation gives an idea for the strength of this mechanism in materials of the SrTiO_3 type for the case where the central symmetry is violated by a polar perturbation.
- ⁴⁰A.K. Tagantsev, Appl. Phys. Lett. **76**, 1182 (2000).
- ⁴¹Landolt-Börnstein, *Numerical Data and Functional Relationships in Science and Technology*, New Series, Vol. III/16 (Springer, Berlin, 1981); Vol. III/29a (Springer, Berlin, 1992).
- ⁴²V.B. Vaks, *Introduction to the Microscopic Theory of Ferroelectrics* (Nauka, Moscow, 1973) (in Russian).
- ⁴³N.A. Pertsev, A.K. Tagantsev, and N. Setter, Phys. Rev. B **61**, R825 (2000).
- ⁴⁴B. Hehlen, Ph.D. thesis, Université Montpellier II, 1995.
- ⁴⁵B. Hehlen, L. Arzel, A.K. Tagantsev, E. Courtens, Y. Inaba, A. Yamanaka, and K. Inoue, Phys. Rev. B **57**, R13 989 (1998).
- ⁴⁶B. Hehlen, L. Arzel, A.K. Tagantsev, E. Courtens, K. Inoue, and A. Yamanaka, Physica B **263-264**, 627 (1999).
- ⁴⁷K.A. Müller, in *Local Properties at Phase Transitions, Proceedings of International School of Physics "Enrico Fermi," Varenna, 1973*, edited by K.A. Müller and A. Rigamonti (North-Holland, Amsterdam, 1976).